JMB

NMR Structure of the Sea Urchin (*Strongylocentrotus purpuratus*) Metallothionein MTA

Roland Riek[1], Bénédicte Prêcheur[1], Yunyuan Wang[2], Elaine A. Mackay[2] Gerhard Wider[1], Peter Güntert[1], Aizhuo Liu[1], Jeremias H. R. Kägi[2] and Kurt Wüthrich[1]*

[1]*Institut für Molekularbiolgie und Biophysik, Eidgenössische Technische Hochschule-Hönggerberg, CH-8093, Zürich Switzerland*

[2]*Biochemisches Institut Universität Zürich CH-8057, Zürich, Switzerland*

*Corresponding author

The three-dimensional structure of [^{113}Cd$_7$]-metallothionein-A (MTA) of the sea urchin *Strongylocentrotus purpuratus* was determined by homonuclear ^{1}H NMR experiments and heteronuclear [^{1}H,^{113}Cd]-correlation spectroscopy. MTA is composed of two globular domains, an N-terminal four-metal domain of the amino acid residues 1 to 36 and a Cd$_4$Cys$_{11}$ cluster, and a C-terminal three-metal domain including the amino acid residues 37 to 65 and a Cd$_3$Cys$_9$ cluster. The structure resembles the known mammalian and crustacean metallothioneins, but has a significantly different connectivity pattern of the Cys-metal co-ordination bonds and concomitantly contains novel local folds of some polypeptide backbone segments. These differences can be related to variations of the Cys sequence positions and thus emphasize the special role of the cysteine residues in defining the structure of metallothioneins, both on the level of the domain architecture and the topology of the metal-thiolate clusters.

© 1999 Academic Press

Keywords: metallothionein; NMR structure; sea urchin; metal-thiolate cluster topology

Introduction

Metallothioneins (MT) are small cysteine-rich proteins with an outstandingly high content of diverse d^{10} metal ions, such as Zn^{2+}, Cu$^+$ and Cd^{2+}, which occur widely in animal and plant tis-

sues and are implicated in a variety of biological processes (Kägi, 1991). For example, they are thought to have an important role in cellular zinc and copper metabolism (Bremner, 1991) and to protect cells and organisms against damage from toxic metal ions (Templeton & Cherian, 1991), free radicals (Thornally & Vasak, 1985) and other electrophilic agents (Yu *et al.*,1995). Significantly increased cellular MT concentrations have been reported in proliferating cells (Studer *et al.*, 1997; Nagel & Vallee, 1995), in some stages of differentiation (De *et al.*, 1991), during embryonal development (Nemer *et al*, 1984; 1991) and in experimental scrapie (Dandoy-Dron *et al.*, 1998). A special form of MT that occurs in normal brain has also been found to specifically inhibit the neurotrophic activities of Alzheimer's disease cortical extract (Uchida *et al.*, 1991).

Much of our understanding of the biological actions of the MTs has come from comparative analysis of the chemical and structural features. All MTs have uniquely folded polypeptide structures specified by the arrangement of the Cys residues in the chain and the coordination preferences of the metal ions. NMR structures have thus far been determined for three mammalian MTs (Arseniev *et al.*, 1988; Braun *et al.*, 1986; Messerle *et al.*, 1990;

Abbreviations used: MT, metallothionein; MTA, MT isoform A of *Strongylocentrotus purpuratus*; MTAα, α-domain of MTA; MTAβ, β-domain of MTA; hMT-2, human MT isoform 2; MT-2α, α-domain of MT-2; MT-2β, β-domain of MT-2; MT-1, lobster or blue crab MT isoform 1; MT-1α, α-domain of MT-1; MT-1β, β-domain of MT-1; NMR, nuclear magnetic resonance; NOE, nuclear Overhauser effect; 2D, two-dimensional; NOESY, NOE spectroscopy; COSY, correlation spectroscopy; TOCSY, total correlation spectroscopy; ppm, parts per million; $^3J_{HN\alpha}$, vicinal spin-spin coupling constant between the backbone amide proton and the α-proton; $^3J_{\alpha\beta}$, vicinal spin-spin coupling constant between the α-proton and one of the β-protons; r.m.s.d., root-mean-square deviation.

Schultze *et al.*, 1988) and two non-mammalian species (Narula *et al.*,1995; Peterson *et al.*, 1996), and a crystal structure of rat MT is also available (Robbins *et al.*, 1991; Braun *et al.*, 1992). All these structures showed that the metal ions bind to Cys sulphur atoms in metal-thiolate clusters. The mammalian MTs contain 20 Cys and bind a total of seven bivalent metal ions (Me(II)), which are partitioned into a $(Me(II))_3 Cys_9$ cluster enfolded by the N-terminal half of the chain (β-domain) and a $(Me(II))_4 Cys_{11}$ cluster enfolded by the C-terminal half (α-domain). The crustacean MTs contains 18 Cys and bind six metal ions, whereby each of two well-separated domains enfolds a $(Me(II))_3 Cys_9$ cluster (Narula *et al.*, 1995; Otvos *et al.*, 1982; Zhu *et al.*, 1994). Yeast MT (Peterson *et al.*, 1996) binds seven univalent d^{10} metal ions in a single metal-thiolate cluster.

The three-dimensional structure of the metallothionein isoform A of the sea urchin *Strongylocentrotus purpuratus* (MTA) reported here further extends our knowledge of this family of proteins. Similar to the mammalian MTs, the sea urchin protein is encoded by three exons, contains 20 Cys and binds seven metal ions, which are partitioned into a four-metal and a three-metal cluster (Wang *et al.*, 1994, 1995). Sea urchin MTA contains essentially the same number of metal-chelating Cys-Cys and Cys-Xxx-Cys motifs as the mammalian MTs (Nemer *et al.*, 1985), but otherwise there is no obvious sequence relationship with the mammalian MTs. In particular, in the mammalian MTs all three Cys-Cys pairs are located in the carboxyl-terminal half of the polypeptide chain, whereas all four Cys-Cys pairs in sea urchin MTA occur in the N-terminal portion. This interchange, which entails an inverted arrangement of the three and four-metal domains in the two proteins (Wang *et al.*, 1995) is postulated to result from inversion of the second and third exons in the mammalian and echinoid MT families (Harlow *et al.*, 1989). Here, the impact of these similarities and differences in the primary structures on chain folding and on the framework of the metal-thiolate clusters is further evaluated by the determination of the complete three-dimensional structure of sea urchin MTA.

Results

The NMR structure determination of sea urchin $[Cd_7^{2+}]$-MTA was performed at pH 7.0 and 15 °C, using ^{113}Cd or ^{112}Cd-labeled recombinant protein samples (Wang *et al.*, 1994, 1995). The NMR spectral analysis and the structural interpretation of the NMR data followed closely the procedures used previously for rabbit MT-2a (Arseniev *et al.*, 1988; Frey *et al.*, 1985; Neuhaus *et al.*, 1984; Wagner *et al.*, 1986a), rat MT-2 (Wörgötter *et al.*, 1987; Schultze *et al.,* 1988) and human MT-2 (Messerle *et al.,* 1990). Therefore, only a short description of the structure determination is presented here.

Resonance assignments

Resonance assignments were obtained by standard procedures based on the observation of sequential NOEs (Wüthrich, 1986). 2D clean-TOCSY (Griesinger *et al.*, 1988), 2D NOESY (Anil Kumar *et al.,* 1980) and 2D E.COSY (Griesinger *et al.*, 1985) experiments were used for spin system identification. The assignments for the backbone amide protons and the carbon-bound hydrogen atoms are complete except for H^N of Asp3, and γCH$_2$ and δCH$_2$ of Lys30 (Figure 1). Among the labile side-chain protons, all amide protons of Asn and Gln residues were assigned, and so was the hydroxyl proton of Thr58. The analysis of the $^3J_{HN\alpha}$ and $^3J_{\alpha\beta}$ coupling constants in combination with the intraresidual and sequential NOEs using the program HABAS (Güntert *et al.*, 1989) yielded stereospecific assignments for 14 βCH$_2$ groups. The ^1H, ^{15}N and ^{113}Cd chemical shifts have been deposited in the Bio Mag Res Bank, accession numbers r1qjkmr and r1qjlmr.

The seven metal ions in sea urchin $[Cd_7^{2+}]MTA$ are labeled I to VII in the order of decreasing chemical shift (Wang *et al.*, 1994). The thiolate-metal connectivities were determined using 2D $[^{113}Cd,^1H]$-COSY spectra (Frey *et al.*, 1985). The distribution of the Cd ions into a four-metal cluster and a three-metal cluster could thus be unambiguously established. Employing the convention adopted for the mammalian MTs (e.g. Messerle *et al.*, 1990) we denote the four-metal domain as ''α-domain'' and the three-metal domain as ''β-domain''. It is to be noted, however, that compared to the mammalian MTs, the sequential arrangement of the two domains is inverted in the sea urchin protein (see Figure 6, below).

Collection of conformational constraints and structure calculation

A total of 1446 NOESY cross-peaks, and 49 $^3J_{HN\alpha}$ and 31 $^3J_{\alpha\beta}$ coupling constants (Figures 1 and 2) were determined and used for the generation of the input constraints for the structure calculation. In addition, there were the constraints for the 28 Cd^{2+}-sulfur bonds (Arseniev *et al.*, 1988). Separate structure calculations were performed for the two domains, since no long-range NOEs were observed between protons located in the different domains. For the β-domain, the input for the final structure calculation with the program DYANA (Güntert *et al.*, 1997) consisted of 234 NOE upper limit distance constraints (58 intraresidual, 69 sequential, 48 medium-range, 59 long-range) and constraints on 12 Cd-S bonds and 60 dihedral angle constraints, for the α-domain there were 420 NOE distance constraints (97 intraresidual, 134 sequential, 97 medium-range, 92 long-range), constraints on 16 Cd-S bonds and 83 dihedral angle constraints. Figure 2 shows that a higher density of NOEs was observed for the α-domain comprising residues 2-36 than for the β-domain of residues 37-64. The standard
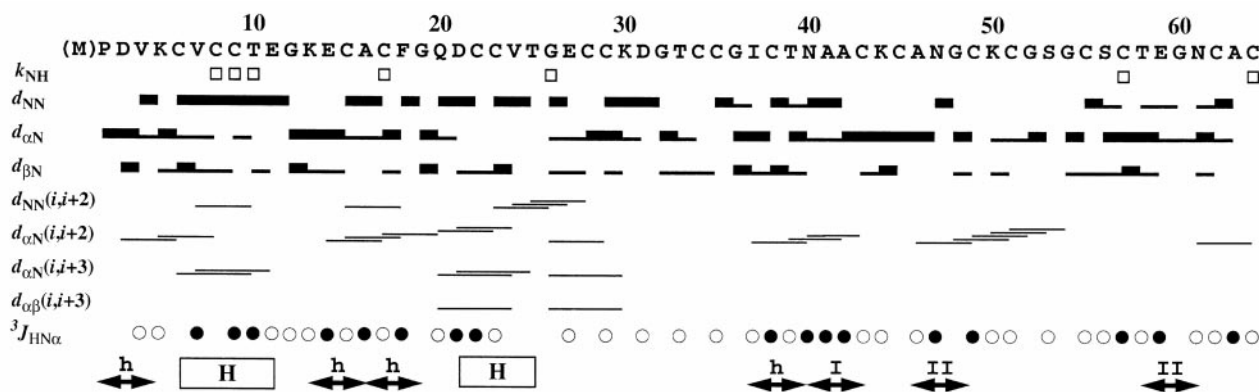
Figure 1. Amino acid sequence of the metallothionein MTA from the sea urchin *Strongylocentrotus purpuratus* (the N-terminal Met is shown in parentheses, since it was absent from the recombinant protein used here) and survey of the sequential and medium-range NOE connectivities, amide proton exchange data and $^3J_{HN\alpha}$ coupling constants. Sequential NOE connectivities d_{NN}, $d_{\alpha N}$ and $d_{\beta N}$ are indicated with thick and thin black bars for strong and weak NOEs, respectively. Medium-range connectivities $d_{NN}(i, i + 2)$, $d_{\alpha N}(i, i + 2)$, $d_{\alpha N}(i, i + 3)$ and $d_{\alpha \beta}(i, i + 3)$ are shown by lines starting and ending at the positions of the two residues related by the NOE. In the row labeled $^3J_{HN\alpha}$, filled and open circles denote residues with $^3J_{HN\alpha} < 6.0$ Hz and $^3J_{HN\alpha} > 7.0$ Hz, respectively. In the row labeled k_{NH}, squares identify residues with sufficiently slow amide proton exchange rates to enable observation of the $^1H^N$-$^1H^\alpha$ cross-peaks in a $^1H,^1H$-TOCSY spectrum recorded 30 minutes after dissolving the protein in ^2H_2O at 15 °C and pH 7.0. Common secondary structure elements are indicated at the bottom, where H indicates helices, I and II indicate turns of types I and II, respectively, and h stands for half-turns (Wagner *et al.*, 1986b).

DYANA torsion angle dynamics protocol was employed (Güntert *et al.*, 1997). The small size and small number of residual constraint violations in the 20 conformers that are used to represent the solution structure show that the input data represent a self-consistent set, and that the constraints are well satisfied in the calculated conformers (Table 1). The high quality of the structure determination is reflected by global r.m.s.d. values relative

to the mean coordinates of about 0.8 Å for the backbone atoms of both domains (Table 1), whereby the core of the α-domain is characterized with greatest precision (Figure 3): the r.m.s.d. calculated for the backbone heavy-atoms of residues 4-30 is 0.4 Å (Table 1). The r.m.s.d. for all heavy-atoms is about 1.2 Å for each domain (Table 1). The arbitrarily predefined tetrahedral metal-Cys connectivities with an allowed metal-sulfur bond length variation of ±0.1 Å are reflected by r.m.s.d. values calculated for the Cys S^γ atoms and the Cd ions of 0.14 Å for the cluster of the α-domain, and 0.27 Å for the β-domain cluster.

The NMR solution structure of sea urchin MTA

As it had become evident during the collection of conformational constraints, the global three-dimensional structure of sea urchin $[Cd_7^{2+}]MTA$ is characterized by the presence of two domains, i.e. an α-domain comprising residues 2-36 and a four-metal cluster (Figure 3(a)), and a β-domain comprising residues 37-64 and a three-metal cluster (Figure 3(b)). No information on the relative spatial orientation of the two domains was obtained from the NMR data, indicating that they are connected only by the flexible linker peptide and not by additional non-bonding contacts that would stabilize a unique docking of the two domains against each other.

The four-metal cluster in the α-domain of MTA contains two fused six-membered rings, where the one containing Cd(IV), Cd(VI) and Cd(VII) is in a boat conformation and the one with Cd(IV), Cd(V) and Cd(VI) in a chair conformation (Figures 3(a) and 4(a)). The backbone of residues 2-36 is wound with left-handed chirality around this cluster
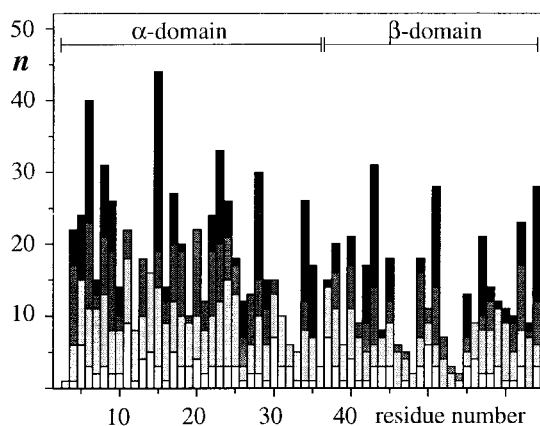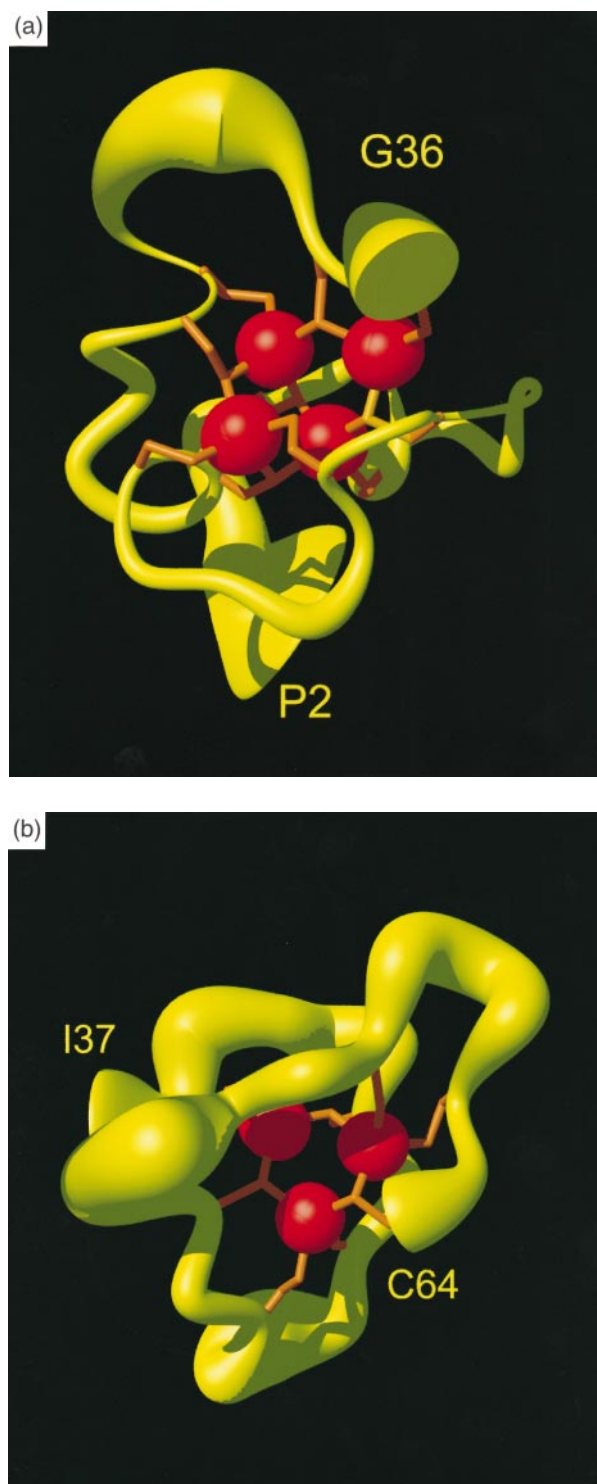

Figure 2. Plot of the number of NOE distance constraints per residue, *n*, *versus* the amino acid sequence of sea urchin MTA (white, intraresidual NOEs; light grey, sequential NOEs; grey, medium-range NOEs; black, long-range NOEs). A total of 97 intraresidual, 134 sequential, 97 medium-range and 92 long-range constraints were determined within the α-domain, and 58 intraresidual, 69 sequential, 48 medium-range and 59 long-range NOE constraints within the β-domain. None of the long-range or medium-range NOEs connect protons in the different domains (see the text).

Table 1. NMR structure determination of sea urchin MTA

Quantity	α-Domain (residues 2-36)	β-Domain (residues 37-64)
DYANA target function (Å²)[a]	1.02 ± 0.23	0.3 ± 0.12
Residual distance constraint violations[a]		
Number ⩾ 0.2 Å	1	1
Sum (Å)	5.1 ± 0.23	1.8 ± 0.4
Maximum (Å)	0.46 ± 0.04	0.24 ± 0.11
Residual dihedral angle constraint violations[a]		
Number ⩾ 5 deg.	0	0
Maximum (deg.)	3.7 ± 0.8	1.3 ± 0.8
Sum (deg.)	18.2 ± 5.5	3.3 ± 2.1
R.m.s.d. to the averaged coordinates[b] (Å)		
N, C^α, C′	0.85 ± 0.17	0.75 ± 0.13
All heavy atoms	1.2 ± 0.1	1.16 ± 0.21
S^γ and Cd atoms[c]	0.14 ± 0.1	0.27 ± 0.1
N, C^α, C′ of residues 4-30	0.4 ± 0.09	
All heavy atoms of residues 4-30	0.86 ± 0.2	

[a] The values given are the mean ± standard deviations among the 20 conformers used to represent the solution structure.

[b] Average coordinates of the 20 conformers after superposition of all listed atoms.

[c] The tetrahedral metal-sulphur connectivities were predefined with a bond length variation of ±0.1 Å.

Figure 3. (a) The α-domain of sea urchin MTA comprising the residues 2-36 and a four-metal/11 Cys cluster. (b) The β-domain of MTA comprising residues 37-64 and a three-metal/nine Cys cluster. The variable radius of the cylindrical rod, which represents the polypeptide backbone by a spline function through the C^α positions, is proportional to the mean global backbone displacement per residue evaluated after superposition of the atoms N, C^α and C′ of the 20 conformers with the smallest residual DYANA target function values. The cysteinyl side-chains and the S^γ-Cd connectivities are shown as red stick models, and the Cd ions as red spheres. The N and C-terminal amino acids of the domains are labeled with the amino acid one-letter code and the sequence number. These and all other colour pictures were prepared with the program MOLMOL (Koradi et al., 1996).

(Figure 3(a)). The residues 4-30 are significantly better defined than the two peripheral segments 2-3 and 31-36 (Figure 3(a)), with a r.m.s.d. value of 0.4(±0.1) Å for the backbone atoms (compare with Table 1). The following secondary structure elements can be identified. Two somewhat irregular helical regions with the residues Cys6-Glu11 and Asp21-Thr25 (Figure 1), where the hydrogen bonds 9CysH^N-O′Cys6, 10ThrH^N-O′Cys6, 24ValH^N-O′Asp21, 25ThrH^N-O′Asp21 and 26GlyH^N-O′Cys22 occur in more than one-third of the 20 DYANA conformers, and three half-turns with the residues Pro2-Lys5, Lys13-Ala16 and Ala16-Gly19 (Figure 1). Half-turns, which were first described in a mammalian MT (Wagner et al., 1986b), differ from the well-known type II turns in that the angle ϕ_{i+2} is −90° instead of +90°, which prevents formation of the type II turn hydrogen bond. An interesting tertiary structure feature is indicated by slow amide proton exchange for the residues Cys8 and Cys17, which might be due to hydrogen bonding with the sulfur atoms of Cys6 and Cys15, respectively (for a description of this type of hydrogen bond, see Robbins et al., 1991).
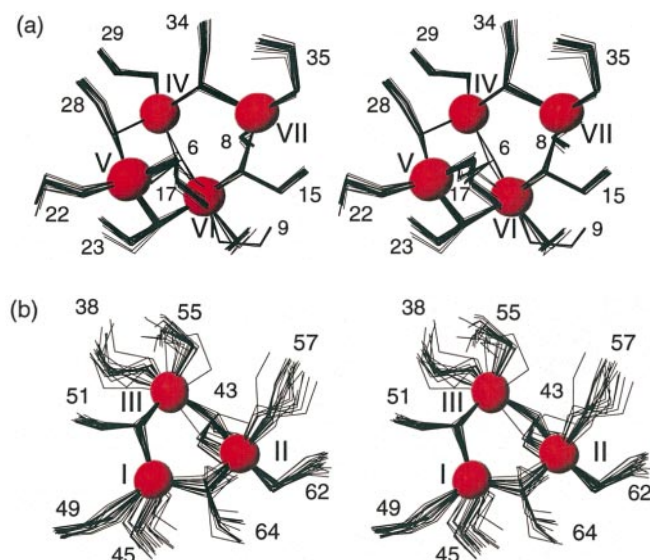
Figure 4. Stereo view of the Cd^{2+}-thiolate clusters in sea urchin MTA. (a) Four-metal cluster of the α-domain; (b) three-metal cluster of the β-domain. The Cd ions are shown as red spheres labeled by roman numerals in the sequence of increasing ^{113}Cd chemical shifts (Wang *et al.*, 1994, 1995). The sulphur-metal coordinative bonds and the cysteine side-chains are shown as black lines representing a superposition of the 20 best DYANA conformers. The sequence positions of the Cys residues are indicated by arabic numerals.

Figure 5. Plot of the sequence of the ratio of the rotating frame relaxation time, $T_{1\rho}$, *versus* the transverse relaxation time, T_2, measured for the backbone amide nitrogen atoms of uniformly ^{15}N-labeled sea urchin $[Cd_7^{2+}]MTA$ at a ^{1}H frequency of 400 MHz. The vertical bars indicate the uncertainty in the measured data. The relaxation rates were determined by least-squares fitting of the magnetization decay curves to a single exponential function. The error bars were obtained by Monte-Carlo type procedures, which involved fitting of the time-course of the peak intensity multiple times with random addition or subtraction of 10 % of the measured peak volume. Where no data are given, spectral overlap prevented reliable measurements.

In the β-domain of MTA the metal-sulfur cluster is in a boat conformation (Figure 4(b)), and the backbone winds around the cluster with left-handed chirality (Figure 3(b)). Common secondary structure elements include two type II turns with Ala46-Cys49 and Thr58-Asn61, for which the hydrogen bonds $49CysH^N$-O′Ala46 and $58ThrH^N$-O′Asn61 were identified with the standard criteria in more than half of the 20 DYANA conformers, a type I turn Asn40-Cys43 with the hydrogen bond $43CysH^N$-O′Asn40, and a half-turn Ile37-Asn40 (Figure 1). The previously identified subtilisin cleavage sites (Wang *et al.*, 1996) are located at this half-turn. Slow amide proton exchange for Cys57 and Cys62 is possibly due to hydrogen bonding with the sulfur atoms of Cys55 and Cys60, respectively.

The lower average number of NOEs per residue in the β-domain of MTA (Figure 2) results in a lower precision of the structure determination for the backbone when compared with the core of the α-domain from residues 4-30 (Table 1). To investigate whether the increased disorder in the β-domain is static or dynamic in nature, we turned to ^{15}N spin relaxation measurements. The $T_{1\rho}/T_2$ ratios (Figure 5) indicate slow conformational exchange on the millisecond to microsecond time-range for the β-domain, whereas the α-domain shows no indication of slow conformational
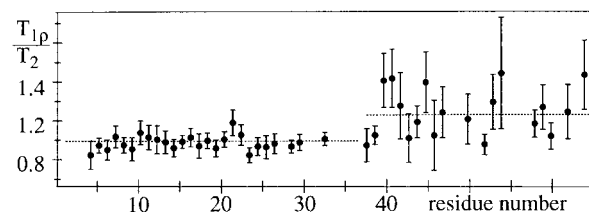
exchange (Szyperski *et al.*, 1993). A similar situation was previously reported for the mammalian MTs, where the NMR-derived structures of the β-domain invariably featured a larger average r.m.s.d. value than the α-domain (Messerle *et al.*, 1990). It has also been shown with ^{113}Cd saturation transfer NMR experiments that the life-time with respect to metal exchange in the three-metal cluster of rabbit MT is shorter than one second, whereas the four-metal cluster domain has corresponding life-times of the order of hours (Otvos *et al.*, 1987, 1989). Thus the conformational exchange process manifested in the ^{15}N relaxation data could be related to the more facile metal exchange in the β-domain. For MTA, a lower limit of about one millisecond for the exchange life-time is given by the fact that well-resolved lines were observed in the ^{113}Cd NMR spectrum (Wang *et al.*, 1994). Both the weaker binding of Cd^{2+} to the β-domain (Wang *et al.*, 1994) and the observed increased dynamic disorder may be a consequence of the smaller number of Cys-metal-Cys crosslinks in the β-domain. With only 18 cross-links, as compared to 24 cross-links in the α-domain, the β-domain might indeed be anticipated to be stabilized to a lesser extent by its total metal complement. However, there is evidence that other factors may play a role. Thus, one of the three-metal clusters in lobster MT-1 was shown to be kinetically more stable than the other (Narula *et al.*, 1995), and amino acid replacements in recombinant mammalian metallothioneins were used to demonstrate that non-cysteine amino acids contribute to the metal-binding competence (Pan *et al.*, 1994; Yamasaki *et al.*, 1997).

Discussion

Structure comparison of sea urchin MTA with human MT-2

Human metallothionein, hMT-2, is used here to represent the three-dimensional structure of mammalian metallothioneins (Messerle *et al.*, 1990). Since the NMR structures of rabbit MT-2a (Arseniev *et al.*, 1988) and rat MT-2 (Schultze *et al.*, 1988), and a crystal structure of rat MT-2 (Braun *et al.*, 1992; Robbins *et al.*, 1991) are all highly similar to that of human MT-2, the resulting conclusions apply to all presently known mammalian MTs.

The dominant impression obtained from comparison of sea urchin $[Cd_7^{2+}]$MTA with h$[Cd_7^{2+}]$MT-2 is that both proteins form a two-domain structure, with one domain containing a three-metal cluster and the other one a four-metal cluster, and that the corresponding individual domains have related geometries in the two proteins. However, the sequential order of the α and β-domains, and hence of the three and four-metal clusters, is inverted between the two MT types. In h$[Cd_7^{2+}]$MT-2 the three-metal-containing β-domain corresponds to the N-terminal half of the sequence and the α-domain is located in the C-terminal part, whereas in sea urchin MTA the N-terminal α-domain contains four metal ions and the C-terminal β-domain three metal ions (Figure 6). This domain inversion confirms inferences from limited proteolysis studies (Wang *et al.*, 1995, 1996) and from comparison of the sea urchin and mammalian gene structures (Harlow *et al.*, 1989; see also Introduction). Combined with the result, obtained with recombinant techniques, that domain inversion in human metallothionein does not influence the Cd-binding affinity (Yamaguchi *et al.*, 1997), the similar metal-binding properties of sea urchin MTA and mammalian MTs indicate that

although the presence of two domains is essential, interdomain interactions have only limited influence on the metal binding by the individual domains.

A superposition of the polypeptide backbone in the human and sea urchin MT α-domains (Figure 7(a)) shows quite similar overall arrangements of the polypeptide chain around the metal-sulfur cluster. This is all the more surprising, since for each of the four pairs of corresponding metal ions (according to Figure 6) the sequence spacings of the Cys ligands differ quite substantially in the two proteins. In particular, this is reflected by the absence of similarity of the structural roles between corresponding cysteine residues in Figure 6, i.e. their serving either as singly bound or bridging ligands. Thus, although there are some similarities in the sequential grouping of the Cys-metal connectivities in sea urchin and human MT, for example, for the pairs of metal ions Cd(IV) in sea urchin MTA and Cd(VII) in hMT2, Cd(VI) and Cd(VI), Cd(VII) and Cd(I), and Cd(V) and Cd(V), the locations of the bridging Cys along the sequence are clearly different. The first cysteine residue of sea urchin MTA, Cys6, is the ligand involved in the special bridged position that belongs to both of the two fused six-membered rings. In hMT-2 this position is occupied by the fourth α-domain cysteine residue, Cys37. The fourth, seventh, eighth and tenth Cys in sea urchin MTA form the additional bridging ligands (Cys15, Cys23, Cys29 and Cys35), whereas in hMT-2 the fourth, sixth, eighth and 11th Cys have this structural role (Cys34, Cys44, Cys50 and Cys60). The last cysteine residue in hMT-2, Cys60, is thus a bridging cysteine residue, whereas Cys35 in MTA is a singly bound ligand. The simple fact that all four metal ions cannot be simultaneously completely overlapped (Figure 7(a)) shows that there must also be some differences between the
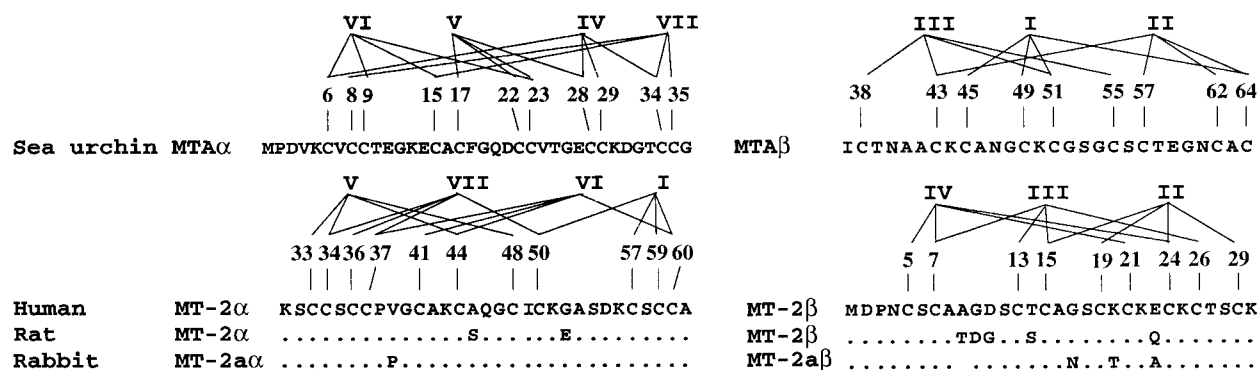

Figure 6. Comparison of the cluster connectivities between the cysteine thiolate groups and the metal ions in the α and β-domains of sea urchin MTA and three mammalian MTs. The metal ions are specified by roman numerals given in the sequence of increasing ^{113}Cd chemical shift (Messerle *et al.*, 1990; Wang *et al.*, 1994, 1995). The amino acid sequences are written in the one-letter amino acid code, where dots for the rat and rabbit proteins indicate identity with the human protein. The coordinative bonds are indicated by straight lines as they were determined by ^{1}H-^{113}Cd or ^{1}H-^{111}Cd heteronuclear correlation experiments (see the text), and the positions of the Cys ligands are given with arabic numerals.
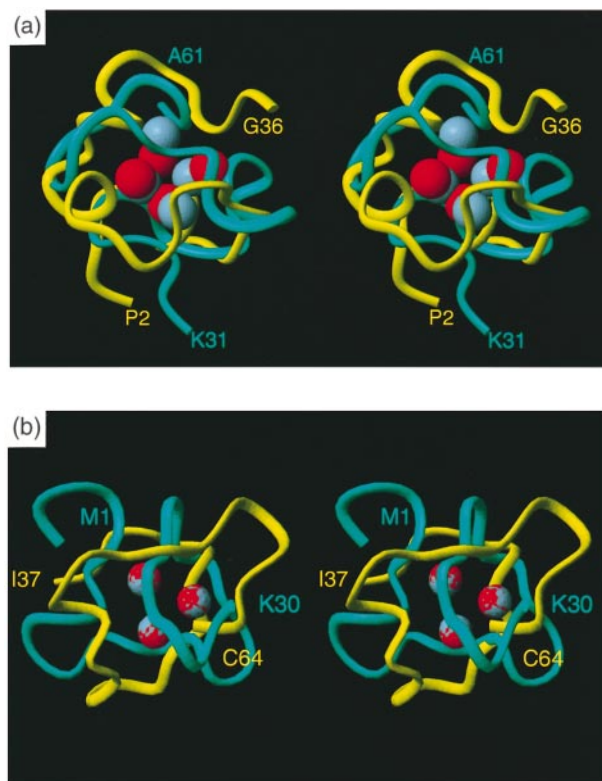
Figure 7. Stereo view of superpositions for best fit of the metal ions of sea urchin MTA and human MT-2. (a) The α-domain; (b) the β-domain. The polypeptide backbone of the sea urchin MTA is drawn as a yellow spline function through the Cα positions, and a corresponding presentation of the backbone of the human MT-2 is shown in cyan. The metal ions are colored red for sea urchin MTA and blue for human MT-2. The terminal amino acid residues of the domains are identified with the one-letter amino acid code and the residue number. The orientation of the MTA structure is approximately the same as in Figure 3.

geometries of the α-domain metal-sulfur clusters in the two species. Indeed, while the two fused six-membered rings of the hMT-2 four-metal cluster both have a distorted boat conformation (Messerle et al., 1990), sea urchin MTA contains one ring in a boat conformation and the other one in a chair conformation (see Results). In view of these differences in structural details, the overall similarity of the polypeptide fold of the α-domains in the two proteins is quite remarkable.

Analogous similarities and dissimilarities can be noticed in the organization of the three-metal clusters of the sea urchin and mammalian proteins (Figure 6). In contrast to all other presently known three-metal cluster-containing MT domains, the chirality of the sea urchin MTA β-domain is left-handed, however. In Figure 7(b) a superposition of the MTA β-domain with the hMT β-domain for best fit superposition of the Cd ions clearly visualizes the opposite chiralities.

Structure comparison of sea urchin MTA with MT-1 of blue crab and lobster

The metal-polypeptide connectivities in the three-metal clusters of these three MTs show again similarities and deviations, but overall there is a closer coincidence with both the α and β-domains in the two MT-1 s than between MTAβ and the β-domains of mammalian MTs (Figure 8). In each pairwise comparison, two bridging Cys are in homologous positions, whereas the third bridging Cys has switched position with one of the nearest singly coordinated Cys. In MTAβ, the second, fifth and ninth Cys in the sequence are bridging ligands, in the MT-1βs these are the second, fifth and eighth Cys, and in the MT-1αs the second, sixth and ninth Cys. This similarity of the distribution of bridging Cys in the three types of three-metal clusters is probably a reflection of the low number of possibilities allowing for the formation of a cyclic metal-thiolate cluster by these short polypeptides, although otherwise quite varied patterns in the Cys connectivities of the individual metal ions are observed (Figure 8).

Surface location of an aromatic ring in sea urchin MTA

Most metallothioneins are devoid of aromatic residues (Kägi, 1993). It is all the more remarkable that the single Phe in the α-domain of MTA is well defined in a fully solvent-exposed location on the protein surface (Figure 9). Inspection of the three-dimensional structure shows that this aromatic ring could not be accommodated in a hydrophobic interior location without major disruption of the
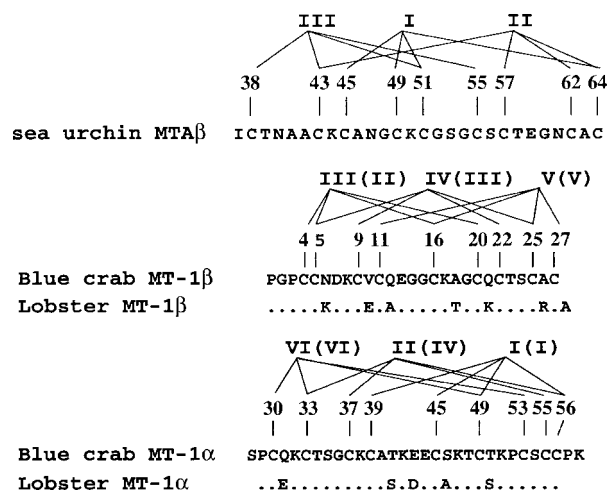

Figure 8. Comparison of the metal-Cys thiolate cluster connectivities in the β-domain of sea urchin MTA and the two three-metal domains of blue crab MT-1 and lobster MT-1. Same presentation as in Figure 6. The roman numerals specifying the metal ions of lobster MT-1 are given in parentheses (note that in each protein the metal ions have been numbered I to VI in the order of decreasing chemical shift).
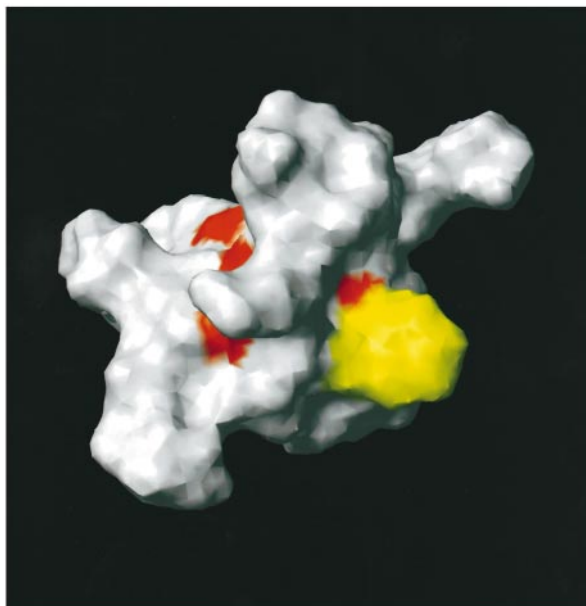
Figure 9. Surface plot of the best DYANA conformer of the α-domain of sea urchin MTA showing the location of Phe18. Color code: Phe, yellow; surface-accessible parts of the metal-thiolate cluster (these are all sulphur atoms), red; others, grey.

metal cluster. It will be of interest to further investigate possible functional or structural roles of this exposed hydrophobic residue, which might, for example, make contacts with the β-domain, with other proteins, or with membraneous particles. In this context, it is of interest that the occurrence of two proline residues in exposed peptide loops of the β-domain in the mammalian MT-3 subclass specifically determines their inhibitory effect on the survival of cortical neurons (Sewell *et al.*, 1995).

General considerations on possible topologies of metal-thiolate clusters connecting three metal ions with nine cysteinyl residues

The schemes in Figures 6 and 8 display a total of eight MT-type three-metal clusters with nine Cys-thiolate ligands. In spite of extensive variation of the Cys sequence positions and numerous amino acid replacements in non-Cys positions, all these MT domains allow for tetrahedral coordination of all three metal ions, with three Cys adopting bridging roles with coordinative bonds to two metal ions. The following additional regularities are observed: (i) the first cysteine residue in the sequence is non-bridging; (ii) the second cysteine residue is a bridging cysteine; (iii) two bridging cysteine residues are always separated by at least one non-bridging Cys (and additional, non-Cys residues); (iv) if two bridging cysteine residues are separated by a single non-bridging Cys, the latter is connected to the same metal ion as its two bridging neighbours. The total number of cluster

topologies (excluding symmetry-related topologies) that satisfy the features (i) - (iv) is 1260. In the following we investigate by structure calculations to what extent this catalogue of possible topologies can be reduced from steric considerations of the three-dimensional protein structures.

Structure calculations were performed with the program DYANA (Güntert *et al.*, 1997), with an input that included the distance constraints used to enforce the tetrahedral geometry around the individual metal ions (Arseniev *et al.*, 1988) and all steric lower distance limits. For each of the 1260 different topologies of the three-metal cluster that satisfy the aforementioned rules (i) - (iv), 16 conformers of the β-domain with the amino acid sequence of sea urchin MTA were calculated, using the standard simulated annealing protocol of DYANA. A topology was considered to be acceptable if the calculation yielded at least one conformer for which all residual violations of the constraints used to enforce the cluster geometry were below 0.015 Å and all violations of steric lower limits below 0.15 Å. This criterion was fulfilled by 462 out of the 1260 possible topologies, including the topologies actually found in sea urchin MTAβ and in the α-domain of the blue crab MT-1. The topologies of human MT-2β and blue crab MT-1β, however, do not satisfy this strict criterion, indicating that they are not compatible with the amino acid sequence of sea urchin MTAβ.

These calculations imply that the Cys arrangement in the sequence still allows for many different topological options. It is then remarkable that no degeneracy of the coordinative bonds is encountered in the presently discussed species. Sea urchin MTA, like the other well-characterised MTs, exists as a unique structure with a fixed topology of the clusters, and with the polypeptide fold conditioned by its particular primary structure. The important role of the Cys sequence positions is emphasized by the fact that numerous non-cysteine residues can be exchanged within a given cluster topology (Figures 6 and 8). Nonetheless, more drastic sequence variations in the non-Cys positions generated by recombinant techniques did in some instances lead to loss of the metal-binding competence (Cody & Huang, 1994; Pan *et al.*, 1994; Yamasaki *et al.*, 1997). On this background, the fact that all 20 cysteine residues and 18 additional non-cysteine residues, including seven glycine residues, are strictly conserved in all eight so far characterized echinoidal MTs (Scudiero *et al.*, 1997) supports the suggestion that these proteins are evolutionarily optimized for efficient metal-thiolate cluster formation, as was found in vertebrate MTs (Kägi, 1993).

General considerations on possible topologies of metal-thiolate clusters connecting four metal ions with 11 cysteinyl residues

The catalogue of possible topologies of metal-thiolate clusters connecting four metal ions with 11

cysteinyl residues is expected to be even larger than for the three-metal clusters, owing to the increased number of metal ions and ligands. Since only two different four-metal cluster topologies are currently known (this work and Messerle *et al.*, 1990), there are not sufficient data to warrant the elaboration of general rules. Therefore, we refrained from a general analysis of four-metal cluster topologies of the type described above for the three-metal clusters. A noteworthy common feature of the two known Cd_4Cys_{11} cluster geometries (Figure 6) is that three of the four Cd ions are coordinated to pairs of sequentially neighboring Cys. In sea urchin MTA, Cd(IV) is connected to Cys28 and Cys29, Cd(V) to Cys22 and Cys23 and Cd(VII) to Cys34 and Cys35 (Figure 6), and in mammalian MTs, Cd(I) is connected to Cys59 and Cys60, Cd(V) to Cys33 and Cys34, and Cd(VII) to Cys36 and Cys37. Interestingly, in all these Cys-Cys dipeptide segments, one Cys serves as a bridging ligand and the other one as a singly bound ligand. There is thus an indication that the involvement of three Cys-Cys dipeptide segments might be essential for the formation of four-metal clusters, and might thus affect the three-dimensional structure of the entire α-domains.

Materials and Methods

Sample preparation

The recombinant polypeptide of sea urchin MTA was expressed in *Escherichia coli* as described (Wang *et al.*, 1994, 1995), and the metalloprotein form was reconstituted either with [113]Cd or with [112]Cd. The NMR measurements were performed at pH 7.0 and 15 °C, using a 3 mM solution of the protein in 90 % H_2O/10 % ^2H_2O with 50 mM NaCl and 20 mM perdeuterated Tris-HCl.

Because the *E. coli* strain 1B 392 D1 used by Wang *et al.* (1994) was not suitable for the production of ^{15}N-labeled protein, *E. coli* strain BL 21(DE 3) grown in slightly modified M63 medium containing 1 g/l of 99 %($^{15}NH_4)_2SO_4$ (Cambridge Isotope Laboratories) and 38 mg/l of ampicillin (Miller, 1993) was used for the expression of ^{15}N-labeled recombinant sea urchin MTA. Cells from 2 l of culture were harvested by centrifugation and were washed using 50 ml of 50 mM Tris-HCl (pH 8.0), containing 0.1 M KCl. The pellet was resuspended in the above buffer containing 3 mM 2-mercaptoethanol and 1 mM PMSF, and passed through a French press at 4 °C. Following addition of streptomycin, the suspension from the broken cells was centrifuged. The further purification included two precipitation steps and fractionation by gel-filtration and ion-exchange chromatography as described (Wang *et al.,* 1994). The yield of ^{15}N-labeled sea urchin MTA was about 1 mg/l of the culture.

For ^{15}N relaxation measurements, a 1.4 mM sample of the ^{15}N-labeled [$^{112}Cd_7$]MTA containing 50 mM NaCl and 20 mM perdeuterated Tris-HCl (pH 7.0) in 90 % H_2O/10 % ^2H_2O was prepared as follows. The solution of the protein in 20 mM Tris-HCl (pH 8.0) was concentrated in an Amicon ultrafiltration cell using a membrane with molecular mass cut-off of 1000 Da. After replacing the unlabelled buffer with a solution of 5 mM NaCl, and

2 mM perdeuterated Tris-HCl (pH 7.0) in a number of successive filtration steps, the resulting sample of volume 5 ml, which contained less than 5 % of the original buffer, was freeze-dried and redissolved in 0.5 ml of 90 % H_2O/10 % ^2H_2O.

NMR spectroscopy

NMR measurements were performed on Bruker AMX500 and AMX600 spectrometers, and on Varian Unity+400 and Unity+750 spectrometers, which are all equipped with three or four radio-frequency channels and probeheads with actively shielded *z*-gradient coils. For data processing and spectral analysis, we used the programs PROSA (Güntert *et al.*, 1992) and XEASY (Bartels *et al.*, 1995), respectively. The ^{1}H chemical shifts are relative to 2,2-dimethyl-2-silapentane-5-sulfonate sodium salt (DSS).

Resonance assignments were obtained by standard procedures (Wüthrich, 1986) from the following homonuclear 2D experiments recorded with [112]Cd-labeled MTA in the absorption mode using TPPI (Marion & Wüthrich, 1983): clean-TOCSY (Griesinger *et al.*, 1988) with $\tau_m = 80$ ms, NOESY with $\tau_m = 60$ ms (Anil Kumar *et al.*, 1980) and E.COSY (Griesinger *et al.*, 1985). The typical data size was 512×2048 complex points in the t_1 and t_2 time-domains, which was then zero-filled to obtain 2048×2048 data points in the spectrum. [$^{113}Cd_7$]MTA was used to obtain a complete set of connectivities between H^β of Cys and Cd^{2+}, using 2D [$^{113}Col,^1H$]-COSY experiments in the absolute value mode with polarization transfer times of 17 ms and 30 ms (Frey *et al.*, 1985). Amide protons with slowed exchange were identified by measuring several clean-TOCSY experiments with a mixing time of 60 ms at different times after dissolving the freeze-dried protein in 99 % ^2H_2O. [15]N spin relaxation time measurements were performed with uniformly ^{15}N-labeled MTA at a ^{1}H resonance frequency of 400 MHz. All [$^{15}N,^1H$]-COSY spectra needed for these measurements were recorded with a time domain data size of 64×1024 complex points, with $t_{1,max}(^{15}N) = 53$ ms and $t_{2,max}(^1H) = 213$ ms. Transverse ^{15}N spin relaxation times, T_2, were obtained from a series of eight spectra as described by Farrow *et al.* (1994), with relaxation delays of 10, 34, 50, 66, 82, 106, 138, and 162 ms. Rotating frame ^{15}N relaxation times, $T_{1\rho}$, were measured using a continuous ^{15}N spin-lock radiofrequency field of 2.5 kHz in a series of nine spectra (Dayie & Wagner, 1994), with relaxation delays of 14, 34, 53, 72, 92, 112, 130, 150, and 170 ms.

Collection of conformational constraints and calculation of the three-dimensional structure

Upper distance constraints were obtained from NOESY cross-peak volumes in the same experiment that was used also for the sequential assignments, which was recorded with a mixing time of 60 ms. The metal-sulfur connectivities were derived from the [$^{113}Cd,^1H$]-COSY data, assuming tetrahedral symmetry for the Cd ions. The distance constraints used to represent the coordinative bonds were the same as described by Arseniev *et al.* (1988). The allowed variation of the metal-sulfur bond length was ± 0.1 Å, the weight of the cluster constraints relative to the NOE constraints was 5. Vicinal $^3J_{\alpha\beta}$ scalar couplings were measured in an E.COSY spectrum, and $^3J_{HN\alpha}$ couplings were determined by inverse Fourier transformation of in-phase multiplets of intraresidual

cross-peaks with the amide protons (Szyperski *et al.*, 1992) in the same NOESY spectrum that was used to obtain upper distance constraints. Dihedral angle constraints and stereospecific assignments for groups of diastereotopic protons were then obtained with the program HABAS (Güntert *et al.*, 1989). The calibration of NOE intensities *versus* ^{1}H-^{1}H distances and the structure calculations were performed with the program DYANA. Other tools of DYANA were used to remove upper distance constraints that represent no effective conformational constraints, and pseudo-atoms with appropriate corrections were introduced where required.

As no conformational constraints could be found between the two domains of the protein, separate structure calculations were done for the β-domain containing residues 1-36, and for the α-domain containing residues 37-64. Several rounds of structure calculations with DYANA and NOESY cross-peak assignment with the program ASNO (Güntert *et al.*, 1993) were performed. The final round of DYANA structure calculations was started with 50 randomized conformers. The 20 DYANA conformers with the smallest target function values were chosen to represent the three-dimensional NMR structure. All colour figures were generated with the program MOLMOL (Koradi *et al.*, 1996).

Calculation of the total number of possible clusters topologies

The number of allowed topologies for a three-metal cluster that are compatible with the rules (i) - (iv) in Results and Discussion was evaluated with an in-house computer program. Starting from all possibilities to connect three bridging and six non-bridging cysteine sulfur atoms to three four-coordinated Cd ions, the program eliminated symmetry-related topologies, and topologies that would violate one of the aforementioned rules (i) - (iv).

Data Bank accession numbers

The atomic coordinates of sea urchin MTA have been deposited with the Brookhaven Protein Data Bank (with accession numbers 1qjk and 1qjl).

Acknowledgements

References

Anil, Kumar, Ernst, R. R. & Wüthrich, K. (1980). A two-dimensional nuclear Overhauser enhancement (2D NOE) experiment for the elucidation of complete proton-proton cross- relaxation networks in biological macromolecules. *Biochem. Biophys. Res. Commun.* **95**, 1-6.

Arseniev, A., Schultze, P., Wörgötter, E., Braun, W., Wagner, G., Vašák, M., Kägi, J. H. R. & Wüthrich, K. (1988). Three-dimensional structure of rabbit liver [Cd$_7$]-metallothionein-2a in aqueous solution determined by nuclear magnetic resonance. *J. Mol. Biol.* **201**, 637-657.

Bartels, C., Xia, T., Billeter, M., Güntert, P. & Wüthrich, K. (1995). The program XEASY for computer-supported NMR spectral analysis of biological macromolecules. *J. Biomol. NMR,* **6**, 1-10.

Braun, W., Wagner, G., Wörgötter, E., Vašák, M., Kägi, J. H. R. & Wüthrich, K. (1986). Polypeptide fold in the two metal clusters of metallothionein-2 by nuclear magnetic resonance in solution. *J. Mol. Biol.* **187**, 125-129.

Braun, W., Vašák, M., Robbins, A. H., Stout, C. D., Wagner, G., Kägi, J. H. R. & Wüthrich, K. (1992). Comparison of the NMR solution structure and the X-ray crystal structure of rat metallothionein-2. *Proc. Natl Acad. Sci. USA,* **89**, 10124-10128.

Bremner, I. (1991). Nutritional and physiological significance of metallothionein. *Methods Enzymol.* **205**, 25-35.

Cody, C. & Huang, P. C. (1994). Replacement of all α-domain lysines with glutamates reduces metallothionein detoxification function. *Biochem. Bipohys. Res. Commun,* **202**, 954-959.

Dandoy-Dron, F., Guillo, F., Benboudjema, L., Deslys, J. P., Lasmezas, C., Dormont, D., Tovey, M. G. & Dron, M. (1998). Gene expression in scrapie. Cloning of a new scrapie- responsive gene and the identification of increased levels of seven other mRNA transcripts. *J. Biol. Chem.* **273**, 7691-7697.

Dayie, K. T. & Wagner, G. (1994). Relaxation-rate measurements for ^{15}N-^{1}H groups with pulsed-field gradients and preservation of coherence pathways. *J. Magn. Reson. ser. A,* **111**, 121-126.

De, S. K., Enders, G. C. & Andrews, G. K. (1991). High levels of metallothionein messenger RNAs in male germ cells of the adult mouse. *Mol. Endocrinol.* **5**, 628-636.

Farrow, N. A., Zhang, O., Forman-Kay, J. D. & Kay, L. E. (1994). A heteronuclear correlation experiment for simultaneous determination of ^{15}N longitudinal decay and chemical exchange rates of systems in slow equilibrium. *J. Biomol. NMR,* **4**, 727-734.

Frey, M. H., Wagner, G., Vašák, M., Sørensen, O. W., Neuhaus, D., Wörgötter, E., Kägi, J. H. R., Ernst, R. R. & Wüthrich, K. (1985). Polypeptide metal cluster connectivities in metallothionein-2 by novel ^{1}H-^{113}Cd heteronuclear two-dimensional NMR experiments. *J. Am. Chem. Soc.* **107**, 6847-6851.

Griesinger, C., Sørensen, O. W. & Ernst, R. R. (1985). Two dimensional correlation of connected NMR transitions. *J. Am. Chem. Soc.* **107**, 6394-6396.

Griesinger, C., Otting, G., Wüthrich, K. & Ernst, R. R. (1988). Clean-TOCSY for ^{1}H spin system identification in macromolecules. *J. Am. Chem. Soc.* **110**, 7870-7872.

Güntert, P., Braun, W., Billeter, M. & Wüthrich, K. (1989). Automated stereospecific ^{1}H NMR assignments and their impact on the precision of protein structure determination in solution. *J. Am. Chem. Soc.* **111**, 3997-4004.

Güntert, P., Dötsch, V., Wider, G. & Wüthrich, K. (1992). Processing of multi-dimensional NMR data with the new software PROSA. *J. Biomol. NMR,* **2**, 619-629.

Güntert, P., Berndt, K. D. & Wüthrich, K. (1993). The program ASNO for computer-supported collection of NOE upper distance constraints as input for protein structure determination. *J. Biomol. NMR,* **3**, 601-606.

Güntert, P., Mumenthaler, Ch. & Wüthrich, K. (1997). Torsion angle dynamics for NMR structure calculation with the new program DYANA. *J. Mol. Biol.* **273**, 283-298.

Harlow, P., Watkins, E., Thornton, R. D. & Nemer, M. (1989). Structure of an ectodermally expressed sea urchin metallothionein gene and characterization of its metal-responsive region. *Mol. Cell. Biol.* **9**, 5445-5455.

Kägi, J. H. R. (1991). Overview of metallothionein. *Methods Enzymol.* **205**, 613-626.

Kägi, J. H. R. (1993). Evolution, structure and chemical activity of class I metallothioneins: an overview. In *Metallothionein III: Biological Roles and Medical Implications* (Suzuki, K. T., Imura, N. & Kimura, M., eds), pp. 29-55, Birkhäuser, Basel.

Koradi, R., Billeter, M. & Wüthrich, K. (1996). MOLMOL: a program for display and analysis of macromolecular structures. *J. Mol. Graph.* **14**, 51-55.

Marion, D. & Wüthrich, K. (1983). Application of phase sensitive two-dimensional correlated spectroscopy (COSY) for measurements of ^{1}H-^{1}H spin-spin coupling constants in proteins. *Biochem. Biophys. Res. Commun.* **113**, 967-974.

Messerle, B. A., Schäffer, A., Vasák, M., Kägi, J. H. R. & Wüthrich, K. (1990). Three-dimensional structure of human [^{113}Cd$_7$]-metallothionein-2 in solution determined by nuclear magnetic resonance spectroscopy. *J. Mol. Biol.* **214**, 765-779.

Miller, J. H. (1993). *Experiments in Molecular Genetics*, 3rd edit., Cold Spring Laboratory Press, Cold Spring Harbor, NY.

Nagel, W. W. & Vallee, B. L. (1995). Cell cycle regulation of metallothionein in human colonic cancer cells. *Proc. Natl Acad. Sci. USA*, **92**, 579-583.

Narula, S. S., Brouwer, M., Hua, Y. & Armitage, I. M. (1995). Three-dimensional solution structure of *Callinectes sapidus* metallothionein-I determined by homonuclear and heteronuclear magnetic resonance spectroscopy. *Biochemistry*, **34**, 620-631.

Nemer, M., Travaglini, E. C., Rondinelli, E. & D'Alonzo, J. (1984). Developmental regulation, induction, and embronic tissue specifity of sea urchin metallothionein gene expression. *Dev. Biol.* **102**, 471-482.

Nemer, M., Wilkinson, D. G., Travaglini, E. C., Sternberg, E. J. & Butt, T. R. (1985). Sea urchin metallothionein sequence: key to an evolutionary diversity. *Proc. Natl Acad. Sci. USA*, **82**, 4992-4994.

Nemer, M., Thornton, R. D., Stuebing, E. W. & Harlow, P. (1991). Structure, spatial and temporal expression of two sea urchin metallothionein genes, SpMTB$_1$ and SpMTA. *J. Biol. Chem.* **266**, 6586-6593.

Neuhaus, D., Wagner, G., Vasák, M., Kägi, J. H. R. & Wüthrich, K. (1984). ^{113}Cd-^{1}H spin- spin couplings in homonuclear ^{1}H correlated spectroscopy of metallothionein: identification of the cysteine ^{1}H spin systems. *Eur. J. Biochem.* **143**, 659-667.

Otvos, J. D., Olafson, R. W. & Armitage, J. M. (1982). Structure of an invertebrate metallothionein form *Scylla serrata*. *J. Biol. Chem.* **257**, 2427-2431.

Otvos, J. D., Engeseth, H. R., Nettesheim, D. G. & Hilt, C. R. (1987). Interprotein metal exchange reactions of metallothionein. In *Metallothionein II* (Kägi, J. H. R. & Kojima, Y., eds), pp. 171-178, Birkhäuser, Basel.

Otvos, J., Chen, S. & Liu, X. (1989). NMR insights into the dynamics of metal interaction with metallothionein. In *Metal Ion Homeostasis: Molecular Biology and Chemistry* (Hamer, D. H. & Winge, D. R., eds), pp. 197-206, Liss, New York.

Pan, P. K., Hou, F., Cody, C. W. & Huang, P. C. (1994). Substitution of glutamic acids for the conserved lysines in the α-domain affects metal binding in both the α and β domains of mammalian metallothionein. *Biochem. Bipohys. Res. Commun.* **202**, 621-628.

Peterson, C. W., Narula, S. S. & Armitage, I. M. (1996). 3D solution structure of copper- and silver-substituted yeast metallothioneins. *FEBS Letters,* **379**, 85-93.

Robbins, A. H., McRee, D. E., Williamson, M., Collett, S. A., Xuong, N. H., Furey, W. F., Wang, B. C. & Stout, C. D. (1991). Refined crystal structure of Cd, Zn metallothionein at 2. 0 Å resolution. *J. Mol. Biol.* **221**, 1260-1293.

Schultze, P., Wörgötter, E., Braun, W., Wagner, G., Vašák, M., Kägi, J. H. R. & Wüthrich, K. (1988). Conformation of [Cd$_7$]-metallothionein-2 from rat liver in aqueous solution determined by nuclear magnetic resonance spectroscopy. *J. Mol. Biol.* **203**, 251-268.

Scudiero, R., Capasso, C., Carginale, V., Riggio, M., Capasso, A., Ciaramella, M., Filosa, S. & Parisi, E. (1997). PCR amplification and cloning of metallothionein complementary DNAs in temperate and antartic sea urchin characterized by a large difference in egg metallothionein content. *Cell. Mol. Life Sci.* **53**, 472-477.

Sewell, A. K., Jensen, L. T., Erickson, J. C., Palmiter, R. D. & Winge, D. R. (1995). Bioactivity of metallothionein-3 correlates with its novel β domain sequence rather than with metal binding properties. *Biochemistry,* **34**, 4740-4747.

Studer, R., Vogt, C. P., Cavigelli, M., Hunziker, P. & Kägi, J. H. R. (1997). Metallothionein accretion in human hepatic cells is linked to cellular proliferation. *Biochem. J.* **328**, 63-97.

Szyperski, T., Güntert, P., Otting, G. & Wüthrich, K. (1992). Determination of scalar coupling constants by inverse Fourier transformation of in-phase multiplets. *J. Magn. Reson.* **99**, 552-560.

Szyperski, T., Luginbühl, P., Otting, G., Güntert, P. & Wüthrich, K. (1993). Protein dynamics studied by rotating frame ^{15}N spin relaxation times. *J. Biomol. NMR,* **3**, 151-164.

Templeton, D. M. & Cherian, M. G. (1991). Toxicological significance of metallothionein. *Methods Enzymol.* **205**, 11-24.

Thornalley, P. J. & Vašák, M. (1985). Possible role for metallothionein in protection against radiation-induced oxidative stress. Kinetics and mechanism of its reaction with superoxide and hydroxyl radicals. *Biochim. Biophys. Acta,* **827**, 36-44.

Uchida, Y., Takio, K., Titani, K., Ihara, Y. & Tomonaga, M. (1991). The growth inhibitory factor that is deficient in the Altzheimer's disease brain is a 68-amino acid metallothionein- like protein. *Neuron,* **7**, 337-347.

Wagner, G., Neuhaus, D., Wörgötter, E., Vasak, M., Kägi, J. H. R. & Wüthrich, K. (1986a). Sequence-specific ^{1}H NMR assignments in rabbit liver metallothionein-2. *Eur. J. Biochem.* **157**, 275-289.

Wagner, G., Neuhaus, D., Wörgötter, E., Vasak, M., Kägi, J. H. R. & Wüthrich, K. (1986b). Nuclear magnetic resonance identification of "half-turn" and 3$_{10}$-helix secondary structure in rabbit liver metallothionein-2. *J. Mol. Biol.* **187**, 131-135.

Wang, Y., Mackay, E. A., Kurasaki, M. & Kägi, J. H. R. (1994). Purification and characterisation of

recombinant sea urchin metallothionein expressed in *Escherichia coli. Eur. J. Biochem.* **225**, 449-457.

Wang, Y., Mackay, E. A., Zerbe, O., Hess, D., Hunziker, P. E., Vašák, M. & Kägi, J. H. R. (1995). Characterization and sequential localization of the metal clusters in sea urchin metallothionein. *Biochemistry,* **34**, 7460-7467.

Wang, Y., Hess, D., Hunziker, P. E. & Kägi, J. H. R. (1996). Separation and characterization of the metal-thiolate-cluster domains of recombinant sea urchin metallothionein. *Eur. J. Biochem.* **241**, 835-839.

Wörgötter, E., Wagner, G., Vašák, M., Kägi, J. H. R. & Wüthrich, K. (1987). Sequence-specific ^{1}H NMR assignments in rat liver metallothionein-2. *Eur. J. Biochem.* **167**, 457-466.

Wüthrich, K. (1986). *NMR of Proteins and Nucleic Acids,* Wiley, New York.

Yamaguchi, R., Kurasaki, M. & Kojima, Y. (1997). A mutant metallothionein which has inverse fragment composition exhibits high cadmium-binding ability. *Biochem. Mol. Biol. Int.* **41**, 49-56.

Yamasaki, F., Kurasaki, M., Oikawa, S., Emoto, T., Okabe, M. & Kojima, Y. (1997). Effects of amino acid replacments on cadmium binding of metallothionein α-fragment. *Cell. Mol. Life Sci.* **53**, 459-465.

Yu, X., Wu, Z. & Fenselau, C. (1995). Covalent sequestration of melphalan by metallothionein and selective alkylation of cysteines. *Biochemistry,* **34**, 3377-3385.

Zhu, Z., DeRose, E. F., Mullen, G. P., Petering, D. H. & Shaw, C. F., III (1994). Sequential proton resonance assignments and metal cluster toplogy of lobster metallothionein-1. *Biochemistry,* **33**, 8858-8865.

Edited by P. E. Wright